European Journal of Medicinal Chemistry 222 (2021) 113600

Contents lists available at ScienceDirect

European Journal of Medicinal Chemistry

journal homepage: http://www.elsevier.com/locate/ejmech

A 2-(benzothiazol-2-yl)-phenolato platinum(II) complex as potential photosensitizer for combating bacterial infections in lung cancer chemotherapy†

Enrique Ortega [a], Cristina Pérez-Arnaiz [b], Venancio Rodríguez [a], Christoph Janiak [c], Natalia Busto [b, **], Begoña García [b, ***], José Ruiz [a, *]

[a] Departamento de Química Inorgánica, Universidad de Murcia and Institute for Bio-Health Research of Murcia (IMIB-Arrixaca), E-30071, Murcia, Spain
[b] Departamento de Química, Facultad de Ciencias, Universidad de Burgos, Plaza Misael Bañuelos S/n, E-09001, Burgos, Spain
[c] Institut für Anorganische Chemie und Strukturchemie, Heinrich-Heine-Universität Düsseldorf, Universitätsstr 1, 40225, Düsseldorf, Germany

ARTICLE INFO

Article history:
Received 4 March 2021
Received in revised form
4 May 2021
Accepted 30 May 2021
Available online 10 June 2021

Keywords:
Platinum(II) complexes
Anticancer and antibacterial activity
Photodynamic inhibition
Photodynamic therapy
Dual action agents

ABSTRACT

Cancer and antibiotic resistance are two global health threats that usually hamper clinical chemotherapeutic efficacy. Particularly for lung cancer, bacterial infections frequently arise thereby complicating the course of cancer treatment. In this sense, three new neutral luminescent cycloplatinated(II) photosensitizers of the type [Pt(dmba)(L)] (dmba = *N*,*N*-dimethylbenzylamine-κ*N*,κ*C*; L = 2-(benzo[*d*]oxazol-2-yl)-phenolato-κ*N*,κ*O* **1**, 2-(benzo[*d*]thiazol-2-yl)-phenolato-κ*N*,κ*O* **2**, and 2-(1-methyl-1H-benzo[*d*]imidazole-2-yl)phenolato-κ*N*,κ*O* **3**) have been characterized and developed to potentially eliminate both resistant bacteria and lung cancer cells. The phototherapeutic effects of complex **2** have been evaluated using low doses of blue light irradiation. Complex **2** exerted promising photoactivity against pathogenic Gram-positive bacteria strains of clinical interest, displaying a phototoxic index (PI) of 15 for methicillin-resistant *Staphylococcus aureus*, one of the major microorganisms predominating lung infections. Likewise, the anticancer activity of **2** was also increased upon light irradiation in human lung A549 cancer cells (PI = 36). Further *in vitro* experiments with this platinum(II) complex suggest that ROS-generating photodynamic reactions were involved upon light irradiation, thus providing a reasonable mechanism for its dual anticancer and antibacterial activities.

1. Introduction

One of the common challenges faced by chemotherapy patients are bacterial infections usually caused by one type of microorganism or by more than one type (polymicrobial infections) due to inherent cancer immunodeficiencies, neutropenia, disruption of mucosal barriers, etc. [1–3]. During the last decades, Gram-positive bacterial infections including those caused by multidrug-resistant (MDR) bacteria such as methicillin-resistant *Staphylococcus aureus* or vancomycin-resistant *Enterococcus* species predominate over Gram-negative bacterial infections [3–6].

Therefore, antibiotics are often prescribed during chemotherapy treatment of cancer disease [7–12]. Regarding the latter, in spite of the success of cisplatin (CDDP), carboplatin, and oxaliplatin in therapy for various solid cancers, problems such as drug-resistance and serious side effects hampered their clinical applications and efficacy [13]. As CDDP exerts anticancer activity via DNA lesions [14], it is important to develop new non-conventional anticancer drugs. Metal complexes provide some unique opportunities compared to organic compounds, having access to modes of action that are not possible with purely organic compounds [15]. Currently, organometallic complexes with intermediate properties between the classical inorganic and organic molecules have recently been considered as promising alternatives not only for cancer therapy but also as antimicrobials because of the high reactivity provided by the three dimensional shape of metal complexes and because the coordination ligands in such complexes can be modulated for their pharmacological properties [16–18]. In particular, C^N ligands offer higher stability of the metal complexes

* Corresponding author.
** Corresponding author.
*** Corresponding author.
E-mail addresses: janiak@uni-duesseldorf.de (C. Janiak), nbusto@ubu.es (N. Busto), begar@ubu.es (B. García), jruiz@um.es (J. Ruiz).

https://doi.org/10.1016/j.ejmech.2021.113600

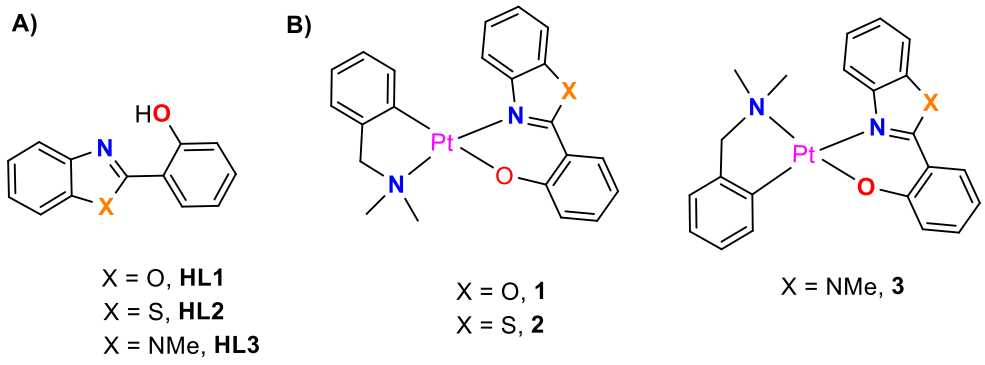

Chart 1. Structures of A) pro-ligands HL and B) new platinum(II) complexes used in this work.

in biological media than most other bidentate ligands, apart from improving their lipophilicity and cellular uptake [16,19–27]. Heterocyclic compounds play essential roles in life and biochemical processes [12,28]. In this sense, the exploitation of possible synergistic effects of the pharmacologically widely used benzimidazole and benzothiazole scaffolds [29–31] with inherent bioactivity and the potential affinity of bioactive metal organometallic complexes [32] is of great interest. Moreover, the behavior of platinum is quite unknown in the field of microbiology and only a few studies of metal complexes have focused on its antibacterial applications [33]. In a recent work Frei *et al.* report the evaluation of metal-containing compounds for antimicrobial activity, among them, five Pt complexes tested were active against methicillin resistant *S. aureus* [33].

On the other hand, light is an outstanding external stimulus of anticancer drugs due to its non-invasive nature and a high level of location and timing control, generating less systemic toxicity for cancer patients and being more effective against resistant cancers [34,35]. The photoactivation could occur either *via* a bond photocleavage reaction (*i.e.*, photoactivated chemotherapy (PACT)) [36–40] or by photodynamic therapy (PDT), the latter involving formation of reactive oxygen species (ROS) through the sensitization of oxygen [41–48]. The octahedral Ru(II) polypyridyl complex (TLD1433) already entered clinical trials as invasive bladder cancer PDT a light-irradiated photosensitizer [46], and a square-planar Pd(II) bacteriopheophorbide (the so-called padeliporfin or WST 11) has been approved for PDT of prostate cancer [49]. An Ir(III)-coumarin derivative able to act as a potent PDT agent against prostate differentiated and tumorigenic cancer stem cells has been recently reported [50]. Similarly, photodynamic microorganism inactivation (PDI) is an interesting strategy that is increasingly used both as therapeutic and as prophylactic modalities for the eradication of MDR bacteria strains [51,52]. It is noteworthy that the photophysical and anticancer properties of some metal complexes bearing benzazolate ligands, and in particular their potential as PDT agents has been recently reported [44,53].

In this context, the development of new compounds provided with antibacterial and antitumor activities that can be easily modulated by photoactivation could be an interesting approach in combating bacterial infections in cancer chemotherapy patients. Herein, we describe the synthesis of three luminescent platinum(II) complexes of the type [Pt(C^N)(L)] (Chart 1), where the deprotonated N,N-dimethylbenzylamine-κN, κC ligand (dmba) remains as the C^N backbone and the chromophoric 2-benzoazole-phenolato N^O ligand has been varied to evaluate the effect on their antibacterial and anticancer activities along with their photopotentiation.

2. Results and discussion

2.1. Synthesis of the new Platinum(II) complexes

A series of neutral cycloplatinated(II) complexes of the type [Pt(dmba)(L)] (Chart 1) containg chromophoric 2-benzoazole-phenolato N^O ligands were prepared from [Pt(dmba)(DMSO)Cl] in moderate to good yields (dmba = N,N-dimethylbenzylamine-κN,κC; HL1 = 2-(2′-hydroxyphenyl)benzoxazole, HL2 = 2-(2′-hydroxyphenyl)benzothiazole, HL3 = 1-methyl-2-(2′-hydroxyphenyl)benzimidazole). Complexes **1**–**3** gave satisfactory elemental analyses and were also characterized by positive-ion ESI-MS ^{1}H, ^{13}C and ^{195}Pt NMR (including COSY, HSQC and HMQC) and UV/Vis spectroscopy (Figs. S1–28). The ^{1}H NMR spectrum of complex **2** in DMSO-d_6 show that both the N-methyl groups and the methylene protons of the dmba are diastereotopic, two separate singlets being observed for the former and two AB doublets for the later (Fig. S8). Therefore, there is no plane of symmetry in the metal coordination plane [21,54]. Furthermore, the aromatic signal of dmba at δ 6.3 ppm is flanked by ^{195}Pt satellites (observed as shoulders). Complex **1** showed broad resonances at 25 °C that sharpens at 75 °C in a reversibly manner (Fig. S22), whereas complex **3** was reactive in DMSO-d_6 even within 10 min at room temperature (Fig. S25). Therefore, NMR characterization of complex **3** was performed in CD_2Cl_2 (^{195}Pt satellites clearly being observed as shoulders) and in DMF-d_7, being stable in this solvent in the absence of light at least for 72 h (Fig. S24). ^{1}H–^{1}H NOESY spectrum of **3** in CD_2Cl_2 showed a NOE cross-peak between the aromatic H^{8} and the NMe groups of the dmba (Fig. S19), indicating that for **3**, in solution, the nitrogen of the imidazole ligand is coordinated trans to C of the dmba (Fig. 1B). However, the same experiment for **1** and **2** in DMSO-d_6 showed NOE cross-peak between H^{8} and the aromatic H^{9} of the dmba (Figs. S5 and S12, respectively). The positive-ion ESI mass spectra of the new complexes exhibited the $[M + H]^+$ signals with the expected isotopic distribution pattern (Figs. S26–S28).

2.2. Crystal structures by X-ray diffraction

Single crystals for X-ray diffraction analysis were obtained for **1** by standing in DMSO-d_6 solution over 3 days, whereas those of **2**

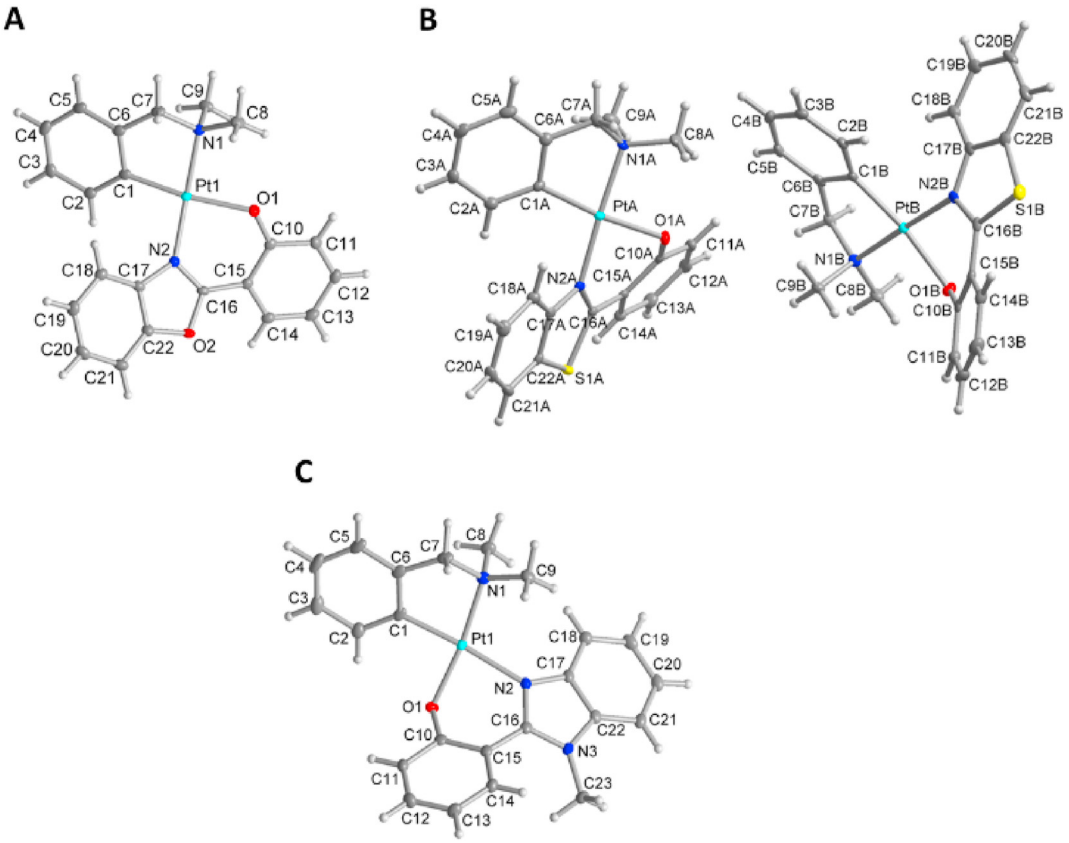

Fig. 1. Molecular structures with atom numbering schemes for (A) **1**, (B) **2**, and (C) **3**·CH_2Cl_2 (CH_2Cl_2 omitted for clarity). Thermal ellipsoids of non-hydrogen atoms are drawn at the 50% probability level. Selected bond lengths and angles for **1**–**3** are shown in the Supporting Information.

and **3**·CH_2Cl_2 were obtained from the slow diffusion of hexane into their corresponding saturated solution in CH_2Cl_2/toluene. The structures of **1**–**3** are shown in Fig. 1. In all cases the Pt atom has a distorted square planar environment, with the C–Pt–N bite angle deviating from 90° due to the bite of the cyclometallated ligand. The Pt–C_{C^N} bond distances lie within the expected range, that is, very close to 2.0 Å [21,23]. Two symmetry-independent molecules of **2** were found here in the structural asymmetric unit. A noteworthy and striking difference in the three molecular structures is the cis/*trans*-positioning of the phenolato group or the N atom of the oxazolyl, thiazolyl or imidazolyl ring relative to the benzylamine ligand (Chart 1). In **1** and **2** the phenolato O atom is trans to the ortho-metallated carbon atom, the N atom of the oxazolyl and thiazolyl is trans to the amine group (Fig. 1A and B). Whereas in **3**·CH_2Cl_2 the phenolato O atom is trans to the amine group and the N atom of the imidazolyl is trans to the ortho-metallated carbon atom (Fig. 1C). The supramolecular packing interactions have been analyzed with PLATON [55]. The packing in **1** is organized mainly by π- π interactions (Fig. S29), whereas the structures of **2** and **3**·CH_2Cl_2 are dominated by C–H···π interactions [56–61] (Figs. S30–S32, respectively and Tables S7–S9) [62]. There are no π - π interactions in **3**·CH_2Cl_2.

2.3. Photophysical and photochemical properties

Absorption and emission spectra of the complexes in aqueous buffered solution at pH = 7.0 are shown in Fig. S33. In general, the absorption spectra of benzazolate complexes are characterized by intraligand transitions (IL). The band at the shorter wavelength is mainly assigned to the π–π* transition of the benzazolate aromatic system [63], and the bands at longer wavelength are attributed to IL transition associated with a charge transfer (CT) from lone pairs of phenolate (donor) to the heterocycle (acceptor). The energy corresponding to this intraligand charge transfer (ILCT) band depends on the metal, its oxidation state and the ligands present in the molecule [64]. As observed the differences in absorption spectra between compounds **1/2** and complex **3** are notably, no absorption being observed above 450 nm for **3**. Bands at λ > 380 nm observed for **1** and **2** could be attributed to spin-allowed metal to ligand (^{1}MLCT, dπ(Pt) → π* [65]. Upon excitation at 375 nm, **1** and **2** show a structured band of emission in the green to orange region centered at 545 and 615 nm, respectively (Fig. S33), and are therefore slightly shifted to longer wavelengths with respect to the free benzazoles (480 and 510 nm for HL1 and HL2, respectively). The emission lifetimes of complexes **1** and **2** are 650 and 970 ns, respectively, in aqueous buffered solution at pH = 7.0, indicating that both complexes are phosphorescent. Complex **3** has a much shorter lifetime (3 ns in aqueous solution), which may be due to the absence of π - π interactions (see above for the crystal structure discussion) due to the NMe substituent. Their emission lifetimes in DMF were much smaller (Table S11). The absorption spectrum of the three complexes in DMF solution at 25 °C (Fig. S34) presented no significant changes over 24 h. However, the UV–vis measurements showed that **3** was not stable in DMSO after 10 min (Fig. S35), as we have

Table 1
MIC values of the studied compounds in the dark and upon 40 min of blue light irradiation (420 nm, 6 J cm^{-2})[a].

–	E. faecium		*S. aureus*	
	Dark	Irradiated	Dark	Irradiated
1	>100	>100	>100	>100
2	5	2	30	2
3	75	75	75	75

[a] Except for *E. faecium*, $t_{irr} = 2$ h

also observed by NMR, whereas no significant changes were observed for **1** and **2** in the same conditions. On the other hand, a big decrease in the intensity of the UV–vis bands was observed for **1** and **3** in aqueous buffered solution containing sodium cacodylate over time (Fig. S36).

2.4. Antibacterial activity

The antibacterial activity of the compounds under study was screened in pathogenic bacteria belonging to the ESKAPE group with a high rate of antibiotic resistance (Table 1 and Table S12). Two Gram-positive (vancomycin-resistant *Enterococcus faecium* and a methicillin-resistant *Staphylococcus aureus*) and two Gram-negative (*Acinetobacter baumanii* and *Pseudomonas aeruginosa*) were employed. The activities of the compounds were expressed as minimal inhibitory concentration (MIC) values *i.e.*, the lowest concentration of the compound that prevents bacterial growth. None of the compounds were active against Gram negative bacteria (MIC values > 100) (Table S12). By contrast, complex **2** was the most active compound against Gram positive strains, thus indicating that the benzothiazole ligand seems crucial for the antibacterial activity, both in the dark and after blue light irradiation. The sulfur atom makes the complex a very potent antimicrobial agent with a remarkable photoactivation in *S. aureus* strain where the photo-index value ($PI = MIC_{irr}/MIC_{dark}$) is 15 after short irradiation periods (Table 1). Thus, **2** can be considered a new promising compound to treat bacterial infections by photodynamic inactivation (PDI).

2.5. Antiproliferative activity and phototoxicity

The antiproliferative activities of platinum complexes were then investigated against a panel of cancer cell lines including lung (A549), colon (SW480) and ovarian (A2780 and A2780cis) cancer cells as well as an in non-tumorigenic ovarian (CHO cells); cisplatin being used as control. None of the ligands were found to be cytotoxic whereas all the studied compounds showed remarkable cytotoxicity against tested tumor cells with half-maximum inhibitory concentration (IC_{50}) values in the low micromolar range (Table S13). The cytotoxicity of the complexes was confirmed in A549 cells by microscopy after 24 h of incubation in the presence of the Pt(II) complexes at the IC_{50} values and 2-fold the IC_{50} values (Fig. S37). Moreover, the platinum compounds were able to overcome cisplatin resistance in A2780cis cell line.

In addition, phototoxicity was evaluated in lung carcinoma A549 cells. First, cell viability was checked after application of visible light alone without complexes, finding that it was not affected (Fig. S38). Low dark toxicity was found in both cancer (A549) and normal (CHO) cells (IC_{50} between 25 and 59) for **1** and **2** (Table 2). However, blue light irradiation on the cellular culture triggered phototoxicity of these compounds as their IC_{50} values significantly decreased, thus rendering phototoxic indices (PI) up to 26 and 36 for **1** and **2**, respectively (Table 2). Such photopotentiation was not observed for **3**, probably due to low absorption of light in this region.

To investigate possible photocleavage effects, a series of experiments applying blue light irradiation to both DMF and cell medium-diluted (DMEM) solutions of the Pt compounds prior treatment was conducted. No differences in IC_{50} between treatments with irradiated and non-irradiated solutions were observed for DMF solutions (Table S14). On the contrary, the IC_{50} values increased when the complexes were pre-irradiated in DMEM. This indicates that species less cytotoxic than **1**–**3** are generated as a consequence of irradiation and, subsequently, that a mechanism such as PACT should be ruled out. However, when **1** and **2** complexes were irradiated with bacteria or cells, in cell medium, a strong increase in cytotoxicity (Tables 1 and 2) was observed, which indicates that these complexes are more active upon irradiation and photostable inside the cells. This led us to conclude that a PDT mechanism would be responsible for the high phototoxic indices (PI) observed.

Overall, the results suggest that sulfur-containing benzothiazole ligand seems to improve the phototherapeutic selectivity of the present compounds and, therefore, **2** was selected for further studies.

2.6. Photo-oxidation of NADH and singlet oxygen quantum yields

In order to shed light on the photopotentiation effects for the best performer **2**, we first observed that after 465 nm blue light irradiation (18 J cm^{-2}), small changes were seen in the UV–vis absorption spectral profile of **2** compared to the sample in the dark in water/DMF (80:20) solution at ambient temperature (Fig. S39), which can be easily related to the deactivation mechanism observed for irradiated solutions in cell culture media (Table S14). Next, we measured its singlet oxygen ($^1O_2$) generation quantum yield (Φ_Δ) in CH_3CN spectroscopically (Fig. S40), obtaining a value of 0.42, which is close to that of the reference $[Ru(bpy)_3]Cl_2$

Table 2
IC_{50} (μM) values obtained for Pt(II) compounds after 1 h incubation, 1 h irradiation with (465 nm, 12.6 J cm^{-2}) and 24 h of cell recovery. Phototoxic indices (PI) are also provided.[a]

Compound		A549	A549 (+NAC)[b]	CHO	PI[c]
1	Dark	57 ± 4	69 ± 5	37 ± 3	
	Irradiated	2.2 ± 0.1	4.2 ± 0.5		26
2	Dark	25 ± 3	26 ± 3	59 ± 4	
	Irradiated	0.69 ± 0.03	1.8 ± 0.1		36
3	Dark	37 ± 6	44 ± 7	13 ± 2	
	Irradiated	22 ± 4	40 ± 4		2

[a] Data expressed as mean values ± SD of three independent experiments (n = 4).
[b] A549 were pretreated with 5 mM of N-acetyl-cysteine (NAC) for 1 h prior treatment schedule.
[c] $PI = [IC_{50}]_{dark}/[IC_{50}]_{irr}$ for A549 cells.

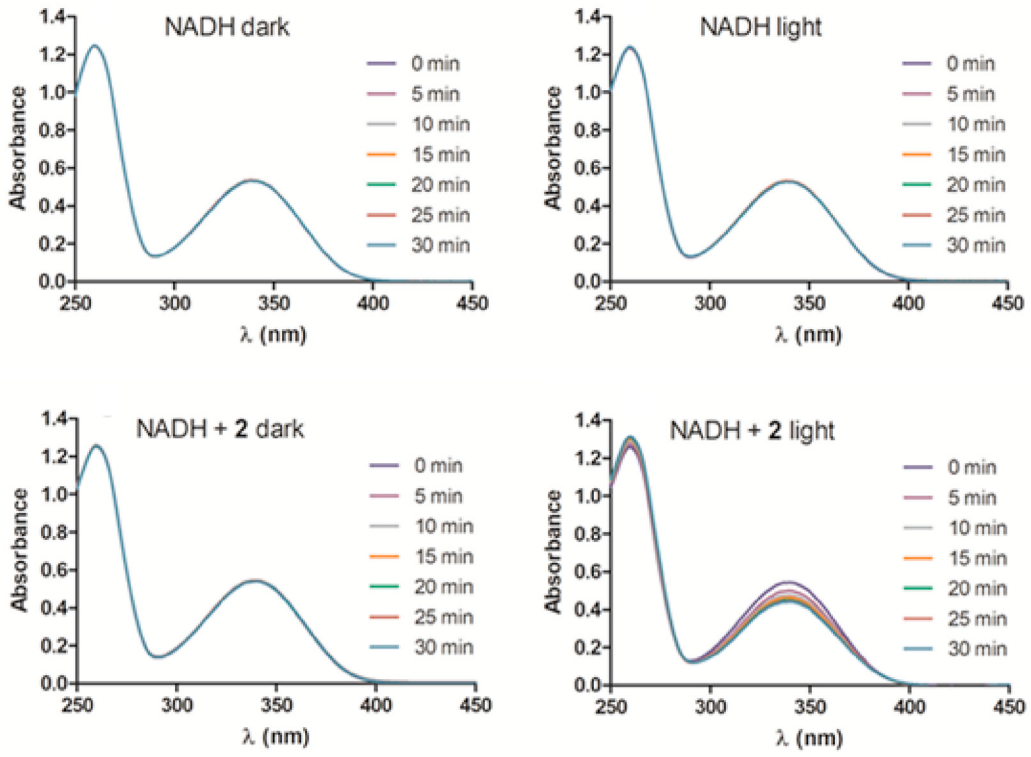

Fig. 2. UV–vis spectra for the photocatalytic oxidation of NADH (100 μM) by complex **2** (5 μM) in a mixture of H_2OmQ/DMF 90/10 (v/v) at 298 K in the dark or under blue light irradiation (465 nm, 18 J cm^{-2}). The NADH oxidation turnover number (TON) was 3.3 after 30 min.

(0.57) [66]. In addition, we explored its catalytic activity for the photo-oxidation of NADH, an important coenzyme in living cells, which participates in the maintenance of the intracellular redox balance in neoplastic tissues [67]. As shown in Fig. 2, complex **2** was photo-catalyst for NADH photo-oxidation as evidenced from the decrease of absorbance of NADH's characteristic band at 339 nm. The turnover frequency (TOF) of **2** for NADH photo-oxidation was 6.6 h^{-1}.

2.7. Cellular accumulation and localization

The luminescence of **1** and **2** allowed us to evaluate cellular localization by confocal microscopy. A549 cells treated with platinum complexes for 0.5 and 3 h exhibited mild to strong intracellular luminescence and showed a punctuated pattern around cell cytoplasm, indicating that compounds were able to rapidly internalize in living cancer cells (Fig. 3A and Fig. S41). This cytoplasmic distribution was corroborated through platinum content determination by ICP-MS (Fig. S42). All the complexes accumulated into A549 cells in a greater extent than cisplatin after 24 h in the dark. Particularly, compound **2** exhibited significantly higher uptake in the non-nuclear fraction compared to **1** and **3** (Fig. 3B).

2.8. Intracellular ROS generation upon light irradiation

Since photo-generation of $^1O_2$ and photo-oxidation catalysis of NADH were observed for complex **2**, we decided to monitor intracellular ROS levels of **2**-treated cancer cells using the fluorescent probe dihydroethidium (DHE), which is oxidized in the presence of ROS thereby intercalating into DNA and exhibiting red fluorescence [68]. Compound **2** (10 μM) increased DHE fluorescence only upon light irradiation, hence indicating its ability for ROS production, while irradiation alone did not result in any observable effects (Fig. 4A and Fig. S43). Moreover, incubation of A549 cells with the well-known ROS scavenger N-acetyl-cysteine (NAC; 5 mM) prior to treatment with compounds attenuated their phototoxic effects, which confirmed that ROS were required for the compounds to act under light irradiation (Table 2 and Fig. S44).

2.9. Morphological changes and apoptosis induction

The ability for **2** to photo-induce cell death prompted us to check the type of cellular damage induced in A549 cells upon irradiation. As shown in Fig. 4B and Fig. S44, under dark conditions **2** rapidly induced morphological changes characterized by nuclear condensation as a reduction in cell size was detected in forward light scatter (FSC) and concomitant transient increase observed in the side scatter (SCC). These morphological changes were also consistent with apoptosis induction, which was further confirmed by flow cytometry (Fig. S45). In contrast, upon 1 h of blue light irradiation, **2** led to dramatic changes in the morphology of A549 cells resulting in an increase of cell size and cell debris that might be ascribable to oxidative damage (Fig. 4B). Overall, these results led us to hypothesize that the phototoxicity of **2** was due to ROS-generating PDT reactions that lead to cellular oxidative damage.

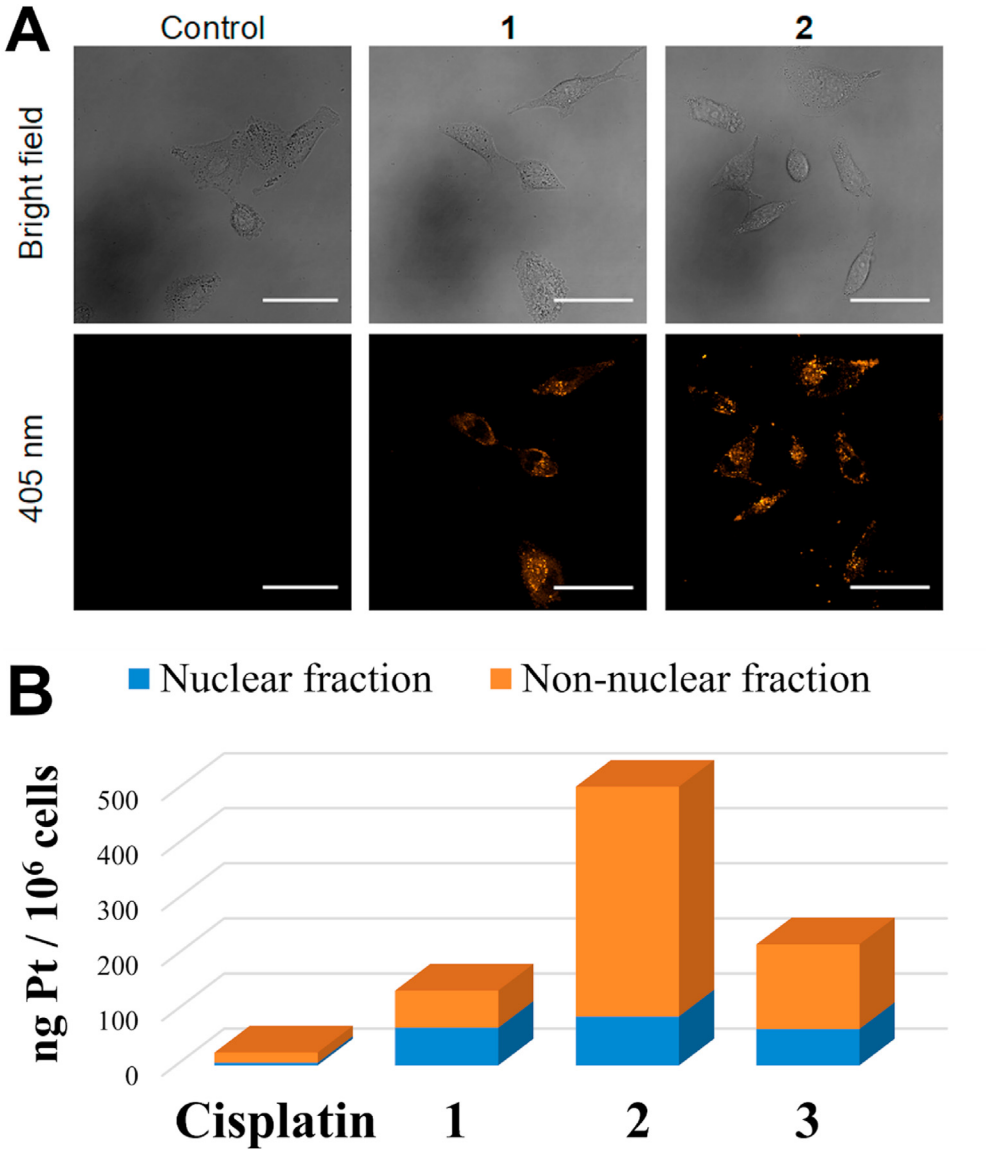

Fig. 3. A) Confocal microscopy images of A549 cells after 0.5 h treatment with **1** and **2** at 10 μM. Scale bar: 50 μm. B) Relative Pt accumulation in the nuclear and non-nuclear fraction of A549 cells exposure to complexes **1**–**3** or cisplatin at 2 μM after 24 h expressed as nanograms of Pt in one million cells.

3. Conclusions

In summary, we report some new neutral luminescent cyclo-platinated(II) 2-benzoazole-phenolato N^O complexes of the type [Pt(dmba)(L)]. Noteworthy, the 2-(benzothiazolyl)phenolato-N,O compound **2** photo-generated $^1O_2$, catalyzed photo-oxidation of NADH and displayed antimicrobial activity against two Gram positive bacteria strains of clinical interest, showing remarkable photoactivity in methicillin-resistant *S. aureus* (PI = 15) upon light irradiation. Complex **2** also exhibited high antiproliferative activity *in vitro* against cancer cells and application of low-doses of blue light (12.6 J cm^{-2}) significantly improved the cytotoxicity against A549 lung carcinoma cells (PI = 36). Additional experiments confirmed intracellular ROS being produced after light irradiation with **2** as well as important changes in cell morphology, which were consistent with its photocytotoxicity. The dual anticancer and antibacterial activity of **2** in the presence of light makes it a promising luminescent platinum PDT candidate for potential elimination of pathogenic multi-resistant bacterial infections in lung cancer chemotherapy.

4. Materials and methods

4.1. General procedures

Unless otherwise noted, preparations were carried out under atmospheric conditions. [Pt(dmba)(DMSO)Cl] and 1-methyl-2-(2′-hydroxyphenyl)benzimidazole (HL3) were prepared using reported procedures [22,69]. HL1, HL2 and all other reagents were obtained from commercial sources and used without further purification.

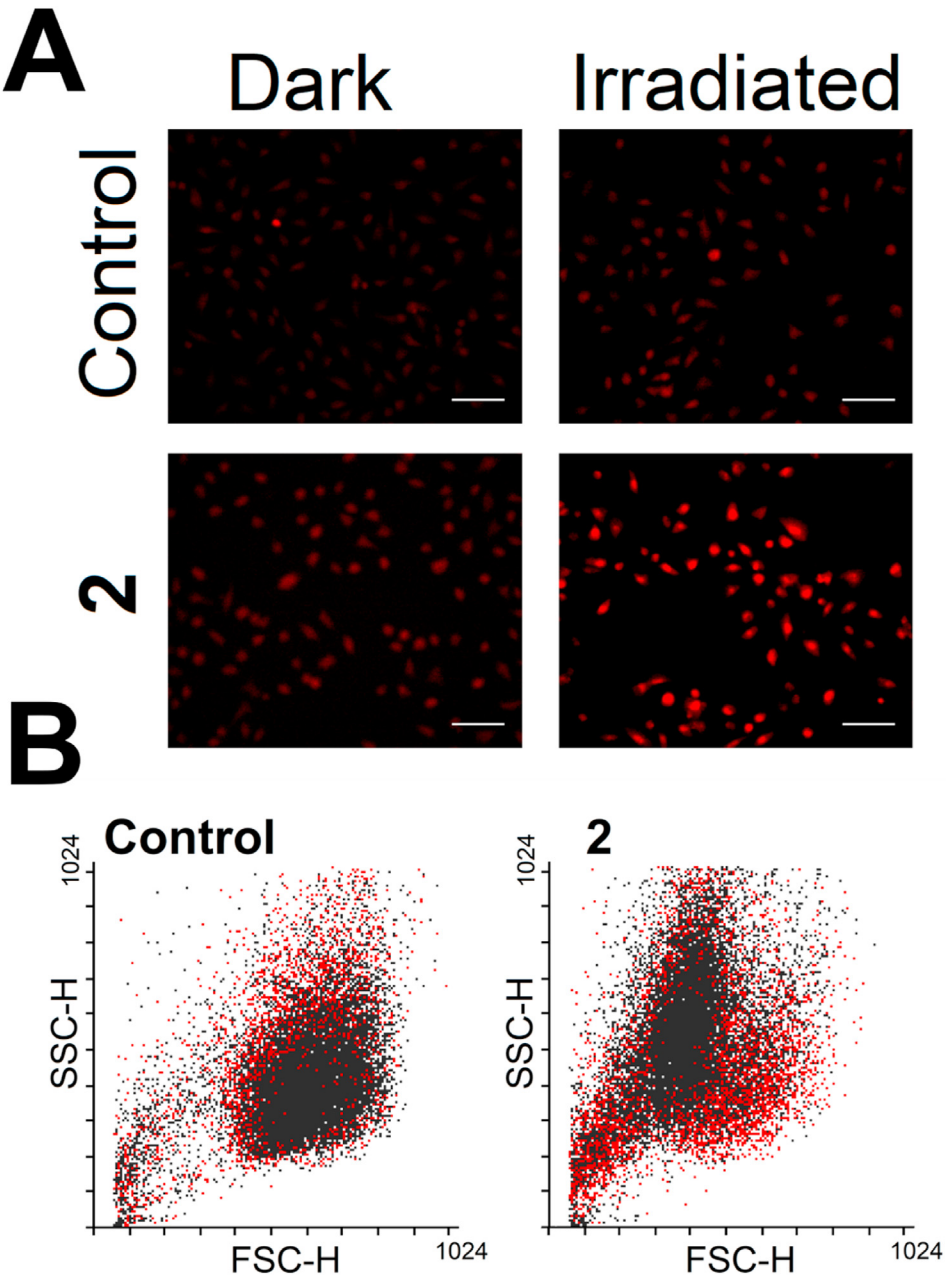

Fig. 4. A) Fluorescent detection of ROS in A549 cells after treatment with **2** (10 μM) in the dark or upon irradiation with blue light (λ = 465 nm, 1 h). Cells were stained with dihydroethidium (DHE) at 10 μM. Scale bar: 100 μm. B) FSC-SSC profiles of A549 cells with (red) and without (black) blue light (λ = 465 nm, 1 h) in the absence or presence of **2** (10 μM).

The C, H, N and S analyses were performed with a Carlo Erba model EA 1108 microanalyzer. The ^{1}H, ^{13}C and ^{195}Pt NMR spectra were recorded on a Bruker AC 300 E or a Bruker AV 400 spectrometer. Chemical shifts are cited relative to $SiMe_4$ (^{1}H and ^{13}C, external) and $Na_2[PtCl_6]$ (^{195}Pt, external). ESI mass analyses were performed on a HPLC/MS TOF 6220. The isotopic distribution of the heaviest set of peaks matched very closely that calculated for the formulation of the complex cation in every case. UV/Vis spectroscopy was carried out on a PerkinElmer Lambda 750 S spectrometer with operating software. Fluorescence measurements were carried out with a PerkinElmer LS 55 50 Hz Fluorescence Spectrometer and Fluorescence Lifetime measurements in a FLS980 equipment (Edinburgh Instruments) in which the photoexcitation was made with a EPL 375 pulse diode laser and the data emission collected was analyzed by FAST 3.4.0 software. Confocal microscopy image processing and display were carried out with ImageJ software.

4.2. Preparation of monomeric Pt(II) compounds 1, 2 and 3

The corresponding 2-benzoazole-phenol HLn (0.23 mmol) was

treated with methanolic KOH (5 mL, 25.81 mg, 0.26 mmol) for 15 min. The resulting solution was treated with a suspension of [Pt(dmba)(DMSO)Cl] (0.1 g, 0.23 mmol) in methanol (15 mL) at room temperature for 48 h (for complexes **1** and **3**) or for 24 h at 65 °C (complex **2**). After removing solvent under reduced pressure, the residue was redissolved by the addition of CH_2Cl_2 (20 mL). The resulting solution was filtered through Celite, and then the solvent was evaporated to dryness. The residue was treated with ether to give a precipitate that was filtered off and air-dried.

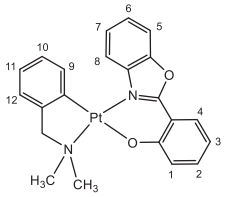

Complex 1. Intense yellow solid. Isolated yield: 65% ^{1}H NMR (300 MHz, DMSO-d_6): δ 7.82–7.75 (m, 2H, H^4+H^5), 7.45–7.37 (m, 2H, H^6+H^7), 7.36–7.26 (m, 2H, H^2+H^8), 7.02 (dd, 1H, H^{12}, J = 7.2, *J* = 0.9 Hz), 6.84 (td, 1H, H^{11}, J = 7.2, *J* = 1.2 Hz), 6.79–6.76 (m, 2H, H^1+H^9), 6.60–6.54 (m, 2H, H^3+H^{10}), 4.11 (s, br, 2H, CH_2N), 2.83 (s, br, 6H, $N(CH_3)_2$). ^{13}C NMR (75.4 MHz, DMSO-d_6): δ 169.2 (Q), 159.0 (Q), 149.2 (Q), 148.9 (Q), 138.5 (Q), 136.0 (CH_1 or CH_9), 134.6 (CH_2 or CH_8), 130.1 (Q), 128.1 (CH_4), 126.1 (CH_6 or CH_7), 124.3 (CH_2 or CH_8), 123.6 (CH_3 or CH_{10}), 123.1 (CH_1 or CH_9), 122.6 (CH_{11}), 121.1 (CH_{12}), 120.0 (CH_6 or CH_7), 114.3 (CH_3 or CH_{10}), 111.3 (CH_5), 111.1 (Q), 74.5 (CH_2N), 50.9 (NCH_3). ^{195}Pt NMR (128.63 MHz, DMSO-d_6): δ −2896.7. ESI-MS (pos. ion mode, DMF): *m*/*z* = 540.12 $[M + H]^+$. Anal. Calcd. for $C_{22}H_{20}N_2O_2Pt$: C, 48.98; H, 3.74; N, 5.19. Found: C, 49.15, H, 3.61; N, 5.02 (%).

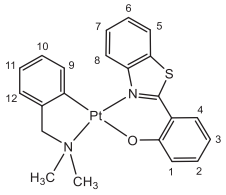

Complex 2. Intense orange solid. Isolated yield: 60%. ^{1}H NMR (400 MHz, DMSO-d_6): δ 8.10–8.08 (m, 1H, H_5), 8.04–8.02 (m, 1H, H_8), 7.52 (dd, 1H, H_4, J = 8.0, *J* = 1.6 Hz), 7.42–7.27 (m, 2H, H_6+H_7), 7.25 (ddd, 1H, H_2, J = 8.4, J = 6.8, *J* = 1.6 Hz), 6.96 (d, 1H, H12, *J* = 7.2 Hz), 6.79–6.76 (m, 2H, H_1+H_{11}), 6.54 (ddd, 1H, H_3, J = 8.0, J = 7.2, *J* = 1.2 Hz), 6.48 (td, 1H, H_{10}, J = 7.6, *J* = 1.2 Hz), 6.29 (dd, 1H, H_9, J = 7.6, *J* = 0.8 Hz), 4.38 (d, 1H, CH_2N, *J* = 13.6 Hz), 3.74 (d, 1H, CH_2N, *J* = 13.6 Hz, Pt satellites are observed as shoulders). 3.07 (s, 3H, NCH_3), 2.56 (s, 3H, NCH_3)·^{13}C NMR (75.4 MHz, DMSO-d_6): δ 169.6 (Q), 167.5 (Q), 151.9 (Q), 150.3 (Q), 137.2 (CH_9), 135.9 (CH_2), 132.7 (Q), 132.4 (Q), 130.6 (CH_4), 127.4 (CH_6 or CH_7), 127.4 (CH_6 or CH_7), 126.7 (CH_5), 125.1 (CH_{10}), 123.9 (CH_1+CH_8+CH_{11}), 122.2 (CH_{12}), 116.2 (CH_3), 75.8 (CH_2N), 52.5 (NCH_3), 52.0 (NCH_3). ^{195}Pt NMR (128.63 MHz, DMSO-d_6): δ −2967.8. ESI-MS (pos. ion mode, DMF): *m*/*z* = 556.10 $[M + H]^+$. Anal. Calcd. for $C_{22}H_{20}N_2OPtS$: C, 47.56; H, 3.63; N, 5.04; S, 5.77. Found: C, 47.65, H, 3.48; N, 4.83; S, 5.88 (%).

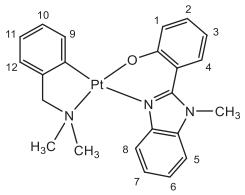

Complex 3. Pale yellow solid. Isolated yield: 56%. ^{1}H NMR (400 MHz, CD_2Cl_2): δ 7.89–7.87 (m, H_8), 7.55–7.51 (m, 2H, H_5+H_9), 7.46–7.39 (m, 3H, H_4+H_6+H_7), 7.17 (ddd, 1H, H_2, J = 8.4, J = 7.2, *J* = 1.6 Hz), 7.06–6.97 (m, 3H, H_{10}+H_{11}+H_{12}), 6.92 (dd, 1H, H_1, J = 8.4, *J* = 1.2 Hz), 6.74 (td, 1H, H_3, J = 8.4, *J* = 1.2 Hz), 3.93 (s, 3H, NCH_3), 3.82 (s, 2H, CH_2N, Pt satellites are observed as shoulders), 3.0 (s, 6H, NCH_3 dmba, JHPt = 33.6 Hz). ^{13}C NMR (100.82 MHz, CD_2Cl_2): δ 171.9 (Q), 151.8 (Q), 148.4 (Q), 140.1 (Q), 137.7 (Q), 137.3 (Q), 132.8 (CH_2), 131.6 (CH_5 or CH_9), 129.2 (CH_4), 124.4 (CH_{10} o CH_{11} or CH_{12}), 123.5 (CH_6+CH_7+ {CH_{10} or CH_{11} or CH_{12}}), 121.5 (CH_1), 120.6 (CH_{10} or CH_{11} or CH_{12}), 119.1 (Q), 117.2 (CH_8), 115.5 (CH_3), 111.2 (CH_5 or CH_9), 77.4 (CH_2N), 55.0 (NCH_3 dmba), 34.0 (NCH_3). ^{195}Pt NMR (128.63 MHz, CD_2Cl_2): δ −2776.31. ESI-MS (pos. ion mode, DMF): *m*/*z* = 553.16 $[M + H]^+$. Anal. Calcd. for $C_{23}H_{23}N_3OPt$: C, 50.00; H, 4.20; N, 7.61. Found: C, 50.08, H, 4.05; N, 7.43 (%).

4.3. X-ray crystal structure analysis

Single crystals for X-ray diffraction analysis were obtained for **1** by standing in DMSO-d_6 solution over 3 days, whereas those of **2** and **3**·CH_2Cl_2 were obtained from the slow diffusion of hexane into their corresponding saturated solution in CH_2Cl_2/toluene/hexane (2:1:3). A summary of crystal data collection and refinement parameters for all compounds are given in Table S1-S6, in the Supporting Information. Crystals were mounted on glass fibres and transferred to the cold gas stream of the diffractometer Bruker Smart APEX. Data were recorded with Mo Kα radiation (λ = 0.71073 Å) in ω scan mode. Absorption correction for the compound was based on multi-scans. The structures were solved by direct methods (SHELXS-97) [70]; refinement was done by full-matrix least squares on F2 using the SHELXLE-2014 program [71]; empirical (multi-scan) absorption correction with SADABS (Bruker) [72]. All non-hydrogen positions were refined with anisotropic temperature factors. Hydrogen atoms for aromatic CH, aliphatic CH_2 and CH_3 groups were positioned geometrically (C–H = 0.95 Å for aromatic CH, C–H = 0.99 Å for CH_2, C–H = 0.98 Å for CH_3) and refined using a riding model (AFIX 43 for aromatic CH, AFIX 23 for CH_2, AFIX 137 for CH_3), with Uiso(H) = 1.2Ueq(CH, CH_2) and Uiso(H) = 1.5Ueq(CH_3). Graphics were drawn with DIAMOND (Version 4.6.2) [73]. The structural data has been deposited with the Cambridge Crystallographic Data Center as CCDC numbers 2007158–2007160 for **1**–**3**, respectively.

4.4. Bacterial strains and antibacterial activity

E. faecium CECT 5253 (vancomycin resistant, Gram positive bacteria) was maintained in Tryptic Soy (TS) broth or agar at 37 °C. *S. aureus* CECT 5190 (methicillin resistant, Gram positive bacteria), *A. baumannii* ATCC 17978 (Gram negative bacteria) and *P. aeruginosa* PAO1 (Gram negative bacteria) were mantained at 37 °C in Mueller-Hinton (MH) broth or agar while *E. faecium*. The antibacterial activity was evaluated by the broth microdilution plate method according to CLSI criteria against ESKAPE (*Enterococcus faecium, Staphylococcus aureus, Klebsiella pneumoniae, Acinetobacter baumannii, Pseudomonas aeruginosa*, and *Enterobacter*

cloacae) pathogens. Briefly, serial dilutions of the compounds were prepared in MHB (1:2 dilutions) in 96-well plates, then plates were inoculated with a final concentration of 5×10^5 CFU/mL. For photoactivation studies, bacteria were irradiated during 2 h with LED blue light (420 nm, 6 J cm^{-2}), except for *S. aureus* that was irradiated 40 min. Then, bacteria were incubated at 37 °C for 18–20 h. The reported Minimum Inhibitory concentrations (MIC) are the mean values from at least two independent experiments with three replicates.

4.5. Cell lines and culture

Human epithelial lung cancer cell line, A549, and Chinese Hamster Ovary cell line, CHO, were grown in F-12 cell medium supplemented with 10% fetal bovine serum (FBS) and 2 mM L-glutamine. SW480 cells were cultured in DMEM supplemented with 10% FBS and and 1% amphotericin-penicillin-streptomycin solution. A2780 and A2780cis cells were grown in RPMI-1640 supplemented with 2 mM Glutamine, 10% FBS and 1% amphotericin-penicillin-streptomycin solution. Cells were maintained in a humidified incubator at 310 K in a 5% CO_2 atmosphere and subcultured twice a week with appropriate density and were confirmed to be mycoplasma-free using Hoechst DNA staining method. A2780cis cells were incubated with 1 μM of cisplatin every 2 passages in order to retain cisplatin resistance.

4.6. MTT antiproliferative assays

SW480, A2780, A2780cis (1×10^4 cells/well) and A549 (5×10^3 cells/well) cells were seeded in 200 μL of their culture medium per well in 96-well plates and incubated at 37 °C under a 5% CO_2 atmosphere for 24 h. Then, cells were treated with different concentrations of the complexes under study and cisplatin as positive control. After treatment, the compounds were removed and cells were incubated with 100 μL of MTT (3-(4,5-dimethyltiazol-2-yl)-2,5-diphenyltetrazoliumbromide) (500 μg/mL). For photocytotoxicity experiments, A549 and CHO cells were seeded for 24 h and incubated with the compounds for 1 h in the dark followed by 1 h incubation under irradiation by placing the Photoreactor EXPO-LED from Luzchem (Canada) fitted with LED Vis lamps (blue lamps λ = 465 nm at a final light6 intensity of 12.6 J cm^{-2}) inside the CO_2 incubator. Irradiated cell culture plates subjected to light irradiation included control cells that were not treated with complexes. Dark control samples were placed in the dark 1 h and then kept in the dark 1 h. Drug-containing medium was then removed by suction, cells washed with PBS and loaded with complete cell medium for 24 h. After cell recovery period, medium was removed and incubated with MTT solution. For photocleavage experiments, high concentrated DMF solutions of the complexes under study were irradiated with blue light irradiation (λ_{irr} = 460 nm, 6.6 J cm^{-2}) for 20 min and 2 h. Then, the MTT Assay was performed with these irradiated solutions after 24 h. After incubation with MTT, 100 μl of solubilizing solution (10% (w/v) SDS, 0.01 M HCl) was added to each well and the absorbance at 570 nm was read in a microplate reader (Cytation 5 Cell Imaging Multi-Mode Reader - Biotek Instruments, USA, and FLUOstar Omega). Four replicates per dose were included and at least two independent experiments were performed. IC_{50} values were calculated from cell survival data using GraphPadPrism Software Inc. version 6.01 (USA).

4.7. Cellular uptake studies by ICP-MS

A549 cells were seeded in 6-well plates at a density of 5×10^5 cells per well and incubated at 37 °C under a 5% CO_2 atmosphere during 24 h. Then, cells were treated with 2 μM of cisplatin and the studied Pt(II) complexes for 24 h. After that, cells were washed twice with DPBS (Dulbecco's Phosphate Buffered Saline) and harvested. Cells were resuspended in 1 mL of DPBS. Cytoplasmic and nuclear fractions were obtained by a fragmentation protocol previously described [74]. Then, samples were diluted with Milli-Q water to obtain 2% HNO_3 solutions. Finally, solutions were analyzed in an 8900 ICP-MS (Agilent Technologies). Data are reported as the mean with the standard deviation of two independent experiments performed by triplicate.

4.8. Photo-oxidation of NADH

The photocatalytic oxidation of NADH by complex **2** was monitored by ultraviolet–visible spectroscopy at 298 K in the dark and under irradiation with blue light (465 nm, 18 J cm^{-2}). The concentration of NADH was obtained using the extinction coefficient at 339 nm (6220 $M^{-1}cm^{-1}$) [75]. TON was defined as the number of moles of NADH that a mol of complex **2** could convert in 30 min. TOF was calculated from the concentration of oxidized NADH (calculated by the difference of concentration of NADH) after 30 min divided by the concentration of complex **2**.

4.9. Confocal microscopy imaging of A549 cells

Briefly, A549 cells were seeded onto Ibidi μ-slide 4 well at a density of $3 \cdot 10^4$ cells/cm^2 and allowed to attach to cell surface. Cells were treated with tested compounds for 0.5 or 3 h at indicated concentrations imaged under confocal microscopy using λ_{exc} = 450 and λ_{em} = 500–600 nm (Leica SP8 systems). Overlay images were obtained with ImageJ software.

4.10. ROS generation assays

The ability of the metal complexes for ROS generation in A549 cells was evaluated using dihydroethidium (DHE) as previously described [76,77]. Briefly, after A549 cells have been allowed to attach the cell surface of 96-well plates ($3 \cdot 10^4$ cells/well), compounds (10 μM) were added following the described schedule for phototoxicity. Then a staining solution (DHE, 10 μM) was loaded into each well for 30 min. The staining was then removed, fluorescence was measured in a FLUOstar Omega spectrophotometer using $\lambda_{exc}/\lambda_{em}$ = 488/620 ± 10 nm (n = 4 replicates) and data analyzed with Microsoft Excel using unpaired *t*-test for statistical significance. Alternatively, A549 cells seeded in 12-well plates followed the same protocol and were imaged in an inverted fluorescence microscope (Zeiss Axio Observer 7) using the red channel.

4.11. Analysis of cell morphology

Cellular morphology analysis of A549 cells after 24 h treatment with platinum complexes was performed using flow cytometry as previously described [74,78]. Briefly, $2 \cdot 10^5$ cells/well were seeded onto 12-well plates and incubated overnight at 37 °C in a humidified incubator with 5% CO_2. Compounds or cisplatin were diluted in medium and added at indicated concentrations following the described light-based treatment schedules (1 h incubation + 1 h irradiation with blue light) or for 24 h. Control cells were treated with the vehicle (0.4% DMF). Cells were then collected by trypsinization, washed with phosphate-buffered saline (PBS), and analyzed by flow cytometry using forward-scattered light (FSC–H) vs side-scattered light (SSC–H) to compare cell size and cell complexity, respectively. Two independent experiments were performed (n = 2 replicates) and data analyzed using Flowing Software 2.5.1 (10^4 events per sample).

Declaration of competing interest

The author declares no competing financial interests.

Acknowledgements

This work was supported by the Spanish Ministerio de Ciencia e Innovación (MCI/AEI) and FEDER funds (Projects RTI2018-096891-B-I00, RTI2018-102040-B-100 and MultiMetDrugs network RED2018-102471-T), Consejería de Educación-Junta de Castilla y León-FEDER (BU042U16-BU305P18), "la Caixa" Banking Foundation (LCF/PR/PR12/11070003) and Fundación Séneca-Región de Murcia (Project 20857/PI/18). E.O. thanks AECC (PRDMU 19003ORTE). Networking support by the COST Action CA18202 is also acknowledged.

Appendix A. Supplementary data

Supplementary data to this article can be found online at https://doi.org/10.1016/j.ejmech.2021.113600.

References

[1] K.V.I. Rolston, G.P. Bodey, A. Safdar, Polymicrobial infection in patients with cancer: an underappreciated and underreported entity, Clin. Infect. Dis. 45 (2007) 228–233, https://doi.org/10.1086/518873.
[2] L.R. Baden, W. Bensinger, M. Angarone, C. Casper, E.R. Dubberke, A.G. Freifeld, R. Garzon, J.N. Greene, J.P. Greer, J.I. Ito, J.E. Karp, D.R. Kaul, E. King, E. Mackler, K.A. Marr, J.G. Montoya, A. Morris-Engemann, P.G. Pappas, K. Rolston, B. Segal, S.K. Seo, S. Swaminathan, M. Naganuma, D.A. Shead, National comprehensive cancer network, prevention and treatment of cancer-related infections, J. Natl. Compr. Canc. Netw. 10 (2012) 1412–1445, https://doi.org/10.6004/jnccn.2012.0146.
[3] H. Liu, S. Long, K.P. Rakesh, G.-F. Zha, Structure-activity relationships (SAR) of triazine derivatives: promising antimicrobial agents, Eur. J. Med. Chem. 185 (2020) 111804, https://doi.org/10.1016/j.ejmech.2019.111804.
[4] S.H. Zinner, Changing epidemiology of infections in patients with neutropenia and cancer: emphasis on gram-positive and resistant bacteria, Clin. Infect. Dis. 29 (1999) 490–494, https://doi.org/10.1086/598620.
[5] E. Montassier, E. Batard, T. Gastinne, G. Potel, M.F. de La Cochetière, Recent changes in bacteremia in patients with cancer: a systematic review of epidemiology and antibiotic resistance, Eur. J. Clin. Microbiol. Infect. Dis. 32 (2013) 841–850, https://doi.org/10.1007/s10096-013-1819-7.
[6] C. Zhao, K.P. Rakesh, L. Ravidar, W.-Y. Fang, H.-L. Qin, Pharmaceutical and medicinal significance of sulfur (SVI)-Containing motifs for drug discovery: a critical review, Eur. J. Med. Chem. 162 (2019) 679–734, https://doi.org/10.1016/j.ejmech.2018.11.017.
[7] X. Zhang, K.P. Rakesh, C.S. Shantharam, H.M. Manukumar, A.M. Asiri, H.M. Marwani, H.-L. Qin, Podophyllotoxin derivatives as an excellent anticancer aspirant for future chemotherapy: a key current imminent needs, Bioorg. Med. Chem. 26 (2018) 340–355, https://doi.org/10.1016/j.bmc.2017.11.026.
[8] B. Moku, L. Ravindar, K.P. Rakesh, H.-L. Qin, The significance of N-methylpicolinamides in the development of anticancer therapeutics: synthesis and structure-activity relationship (SAR) studies, Bioorg. Chem. 86 (2019) 513–537, https://doi.org/10.1016/j.bioorg.2019.02.030.
[9] P. Dong, K.P. Rakesh, H.M. Manukumar, Y.H.E. Mohammed, C.S. Karthik, S. Sumathi, P. Mallu, H.-L. Qin, Innovative nano-carriers in anticancer drug delivery-a comprehensive review, Bioorg. Chem. 85 (2019) 325–336, https://doi.org/10.1016/j.bioorg.2019.01.019.
[10] K.P. Rakesh, H.K. Kumara, H.M. Manukumar, D. Channe Gowda, Anticancer and DNA binding studies of potential amino acids based quinazolinone analogs: synthesis, SAR and molecular docking, Bioorg. Chem. 87 (2019) 252–264, https://doi.org/10.1016/j.bioorg.2019.03.038.
[11] C. Zhao, K.P. Rakesh, S. Mumtaz, B. Moku, A.M. Asiri, H.M. Marwani, H.M. Manukumar, H.-L. Qin, Arylnaphthalene lactone analogues: synthesis and development as excellent biological candidates for future drug discovery, RSC Adv. 8 (2018) 9487–9502, https://doi.org/10.1039/C7RA13754K.
[12] K.P. Rakesh, C.S. Shantharam, M.B. Sridhara, H.M. Manukumar, H.-L. Qin, Benzisoxazole: a privileged scaffold for medicinal chemistry, MedChemComm 8 (2017) 2023–2039, https://doi.org/10.1039/C7MD00449D.
[13] L. Kelland, The resurgence of platinum-based cancer chemotherapy, Nat. Rev. Canc. 7 (2007) 573–584, https://doi.org/10.1038/nrc2167.
[14] T.C. Johnstone, K. Suntharalingam, S.J. Lippard, The next generation of platinum drugs: targeted Pt(II) agents, nanoparticle delivery, and Pt(IV) prodrugs, Chem. Rev. 116 (2016) 3436–3486, https://doi.org/10.1021/acs.chemrev.5b00597.
[15] G. Gasser, N. Metzler-Nolte, The potential of organometallic complexes in medicinal chemistry, Curr. Opin. Chem. Biol. 16 (2012) 84–91, https://doi.org/10.1016/j.cbpa.2012.01.013.
[16] N. Cutillas, G.S. Yellol, C. de Haro, C. Vicente, V. Rodríguez, J. Ruiz, Anticancer cyclometalated complexes of platinum group metals and gold, Coord. Chem. Rev. 257 (2013) 2784–2797, https://doi.org/10.1016/j.ccr.2013.03.024.
[17] M.J. Chow, M.V. Babak, K.W. Tan, M.C. Cheong, G. Pastorin, C. Gaiddon, W.H. Ang, Induction of the endoplasmic reticulum stress pathway by highly cytotoxic organoruthenium schiff-base complexes, Mol. Pharm. 15 (2018) 3020–3031, https://doi.org/10.1021/acs.molpharmaceut.8b00003.
[18] E. Ortega, J. Yellol, M. Rothemund, F.-J. Ballester, V. Rodríguez, G. Yellol, C. Janiak, R. Schobert, J. Ruiz, A new C,N-cyclometalated osmium(II) arene anticancer scaffold with a handle for functionalization and antioxidative properties, Chem. Commun. (2018), https://doi.org/10.1039/C8CC06427J.
[19] E. Lalinde, R. Lara, I.P. López, M.T. Moreno, E. Alfaro-Arnedo, J.G. Pichel, S. Piñeiro-Hermida, Benzothiazole-based cycloplatinated chromophores: synthetic, optical, and biological studies, Chemistry 24 (2018) 2440–2456, https://doi.org/10.1002/chem.201705267.
[20] T. Zou, J. Liu, C.T. Lum, C. Ma, R.C.-T. Chan, C.-N. Lok, W.-M. Kwok, C.-M. Che, Luminescent cyclometalated platinum(II) complex forms emissive intercalating adducts with double-stranded DNA and RNA: differential emissions and anticancer activities, Angew. Chem. Int. Ed. 53 (2014) 10119–10123, https://doi.org/10.1002/anie.201405384.
[21] A. Zamora, S.A. Pérez, M. Rothemund, V. Rodríguez, R. Schobert, C. Janiak, J. Ruiz, Exploring the influence of the aromaticity on the anticancer and antivascular activities of organoplatinum(II) complexes, Chemistry 23 (2017) 5614–5625, https://doi.org/10.1002/chem.201700717.
[22] A. Zamora, S.A. Pérez, V. Rodríguez, C. Janiak, G.S. Yellol, J. Ruiz, Dual antitumor and antiangiogenic activity of organoplatinum(II) complexes, J. Med. Chem. 58 (2015) 1320–1336, https://doi.org/10.1021/jm501662b.
[23] A. Zamora, E. Wachter, M. Vera, D.K. Heidary, V. Rodríguez, E. Ortega, V. Fernández-Espín, C. Janiak, E.C. Glazer, G. Barone, J. Ruiz, Organoplatinum(II) complexes self-assemble and recognize AT-rich duplex DNA sequences, Inorg. Chem. 60 (2021) 2178–3287, https://doi.org/10.1021/acs.inorgchem.0c02648.
[24] Y. Zhu, M. Zhang, L. Luo, M.R. Gill, C. De Pace, G. Battaglia, Q. Zhang, H. Zhou, J. Wu, Y. Tian, X. Tian, NF-κB hijacking theranostic Pt(II) complex in cancer therapy, Theranostics 9 (2019) 2158–2166, https://doi.org/10.7150/thno.30886.
[25] M.V. Babak, M. Pfaffeneder-Kmen, S.M. Meier-Menches, M.S. Legina, S. Theiner, C. Licona, C. Orvain, M. Hejl, M. Hanif, M.A. Jakupec, B.K. Keppler, C. Gaiddon, C.G. Hartinger, Rollover cyclometalated bipyridine platinum complexes as potent anticancer agents: impact of the ancillary ligands on the mode of action, Inorg. Chem. 57 (2018) 2851–2864, https://doi.org/10.1021/acs.inorgchem.7b03210.
[26] D. Nieto, S. Bruña, A.M. González-Vadillo, J. Perles, F. Carrillo-Hermosilla, A. Antiñolo, J.M. Padrón, G.B. Plata, I. Cuadrado, Catalytically generated ferrocene-containing guanidines as efficient precursors for new redox-active heterometallic platinum(II) complexes with anticancer activity, Organometallics 34 (2015) 5407–5417, https://doi.org/10.1021/acs.organomet.5b00751.
[27] A. Kergreis, R.M. Lord, S.J. Pike, Influence of ligand and nuclearity on the cytotoxicity of cyclometallated C^N^C platinum(II) complexes, Chem. Eur J. 26 (2020) 14938–14946, https://doi.org/10.1002/chem.202002517.
[28] M. Xu, Y. Peng, L. Zhu, S. Wang, J. Ji, K.P. Rakesh, Triazole derivatives as inhibitors of Alzheimer's disease: current developments and structure-activity relationships, Eur. J. Med. Chem. 180 (2019) 656–672, https://doi.org/10.1016/j.ejmech.2019.07.059.
[29] J. Yellol, S.A. Pérez, A. Buceta, G. Yellol, A. Donaire, P. Szumlas, P.J. Bednarski, G. Makhloufi, C. Janiak, A. Espinosa, J. Ruiz, Novel C,N-cyclometalated benzimidazole ruthenium(II) and iridium(III) complexes as antitumor and antiangiogenic agents: a structure–activity relationship study, J. Med. Chem. 58 (2015) 7310–7327, https://doi.org/10.1021/acs.jmedchem.5b01194.
[30] G.S. Yellol, J.G. Yellol, V.B. Kenche, X.M. Liu, K.J. Barnham, A. Donaire, C. Janiak, J. Ruiz, Synthesis of 2-Pyridyl-benzimidazole iridium(III), ruthenium(II), and platinum(II) complexes. Study of the activity as inhibitors of amyloid-β aggregation and neurotoxicity evaluation, Inorg. Chem. 54 (2015) 470–475, https://doi.org/10.1021/ic502119b.
[31] H.G. Ghalehshahi, S. Balalaie, H.R. Sohbati, H. Azizian, M.S. Alavijeh, Synthesis, CYP 450 evaluation, and docking simulation of novel 4-aminopyridine and coumarin derivatives, Archiv Der Pharmazie 352 (2019) 1800247, https://doi.org/10.1002/ardp.201800247.
[32] V. Marchan, A. Zamora, A. Gandioso, A. Massaguer, S. Buenestado, C. Calvis, J.L. Hernández, F. Mitjans, V. Rodríguez, J. Ruiz, Towards novel angiogenesis inhibitors based on the conjugation of organometallic platinum(II) complexes to RGD peptides, ChemMedChem 13 (2018) 1755–1762, https://doi.org/10.1002/cmdc.201800282.
[33] A. Frei, J. Zuegg, A.G. Elliott, M. Baker, S. Braese, C. Brown, F. Chen, C.G. Dowson, G. Dujardin, N. Jung, A. Paden King, A.M. Mansour, M. Massi, J. Moat, H.A. Mohamed, A.K. Renfrew, P.J. Rutledge, P.J. Sadler, M.H. Todd, C.E. Willans, J.J. Wilson, M.A. Cooper, M.A.T. Blaskovich, Metal complexes as a promising source for new antibiotics, Chem. Sci. 11 (2020) 2627–2639, https://doi.org/10.1039/C9SC06460E.
[34] X. Wang, X. Wang, S. Jin, N. Muhammad, Z. Guo, Stimuli-responsive therapeutic metallodrugs, Chem. Rev. 119 (2019) 1138–1192, https://doi.org/10.1021/acs.chemrev.8b00209.
[35] A.S. Lubbe, Q. Liu, S.J. Smith, J.W. de Vries, J.C.M. Kistemaker, A.H. de Vries,

I. Faustino, Z. Meng, W. Szymanski, A. Herrmann, B.L. Feringa, Photoswitching of DNA hybridization using a molecular motor, J. Am. Chem. Soc. 140 (2018) 5069–5076, https://doi.org/10.1021/jacs.7b09476.
[36] A. Zamora, C.A. Denning, D.K. Heidary, E. Wachter, L.A. Nease, J. Ruiz, E.C. Glazer, Ruthenium-containing P450 inhibitors for dual enzyme inhibition and DNA damage, Dalton Trans. 46 (2017) 2165–2173, https://doi.org/10.1039/C6DT04405K.
[37] S. Bonnet, Why develop photoactivated chemotherapy? Dalton Trans. 47 (2018) 10330–10343, https://doi.org/10.1039/C8DT01585F.
[38] A. Li, C. Turro, J.J. Kodanko, Ru(II) polypyridyl complexes derived from tetradentate ancillary ligands for effective photocaging, Acc. Chem. Res. 51 (2018) 1415–1421, https://doi.org/10.1021/acs.accounts.8b00066.
[39] M. Lari, M. Martínez-Alonso, N. Busto, B.R. Manzano, A.M. Rodríguez, M.I. Acuña, F. Domínguez, J.L. Albasanz, J.M. Leal, G. Espino, B. García, Strong influence of ancillary ligands containing benzothiazole or benzimidazole rings on cytotoxicity and photoactivation of Ru(II) arene complexes, Inorg. Chem. 57 (2018) 14322–14336, https://doi.org/10.1021/acs.inorgchem.8b02299.
[40] C. Vallotto, E. Shaili, H. Shi, J.S. Butler, C.J. Wedge, M.E. Newton, P.J. Sadler, Photoactivatable platinum anticancer complex can generate tryptophan radicals, Chem. Commun. 54 (2018) 13845–13848, https://doi.org/10.1039/C8CC06496B.
[41] M. Jakubaszek, B. Goud, S. Ferrari, G. Gasser, Mechanisms of action of Ru(II) polypyridyl complexes in living cells upon light irradiation, Chem. Commun. 54 (2018) 13040–13059, https://doi.org/10.1039/C8CC05928D.
[42] T. Chatzisideri, S. Thysiadis, S. Katsamakas, P. Dalezis, I. Sigala, T. Lazarides, E. Nikolakaki, D. Trafalis, O.A. Gederaas, M. Lindgren, V. Sarli, Synthesis and biological evaluation of a Platinum(II)-c(RGDyK) conjugate for integrin-targeted photodynamic therapy, Eur. J. Med. Chem. 141 (2017) 221–231, https://doi.org/10.1016/j.ejmech.2017.09.058.
[43] R.E. Doherty, I.V. Sazanovich, L.K. McKenzie, A.S. Stasheuski, R. Coyle, E. Baggaley, S. Bottomley, J.A. Weinstein, H.E. Bryant, Photodynamic killing of cancer cells by a Platinum(II) complex with cyclometallating ligand, Sci. Rep. 6 (2016) 1–9, https://doi.org/10.1038/srep22668.
[44] M. Martínez-Alonso, N. Busto, L.D. Aguirre, L. Berlanga, M.C. Carrión, J.V. Cuevas, A.M. Rodríguez, A. Carbayo, B.R. Manzano, E. Ortí, F.A. Jalón, B. García, G. Espino, Strong influence of the ancillary ligand over the photodynamic anticancer properties of neutral biscyclometalated IrIII complexes bearing 2-benzoazole-phenolates, Chem. Eur J. 24 (2018) 17523–17537, https://doi.org/10.1002/chem.201803784.
[45] A. Zamora, G. Vigueras, V. Rodríguez, M.D. Santana, J. Ruiz, Cyclometalated iridium(III) luminescent complexes in therapy and phototherapy, Coord. Chem. Rev. 360 (2018) 34–76, https://doi.org/10.1016/j.ccr.2018.01.010.
[46] S. Monro, K.L. Colón, H. Yin, J. Roque, P. Konda, S. Gujar, R.P. Thummel, L. Lilge, C.G. Cameron, S.A. McFarland, Transition metal complexes and photodynamic therapy from a tumor-centered approach: challenges, opportunities, and highlights from the development of TLD1433, Chem. Rev. 119 (2019) 797–828, https://doi.org/10.1021/acs.chemrev.8b00211.
[47] X.-Q. Zhou, M. Xiao, V. Ramu, J. Hilgendorf, X. Li, P. Papadopoulou, M.A. Siegler, A. Kros, W. Sun, S. Bonnet, The self-assembly of a cyclometalated palladium photosensitizer into protein-stabilized nanorods triggers drug uptake in vitro and in vivo, J. Am. Chem. Soc. 142 (2020) 10383–10399, https://doi.org/10.1021/jacs.0c01369.
[48] X.-Q. Zhou, A. Busemann, M.S. Meijer, M.A. Siegler, S. Bonnet, The two isomers of a cyclometallated palladium sensitizer show different photodynamic properties in cancer cells, Chem. Commun. 55 (2019) 4695–4698, https://doi.org/10.1039/C8CC10134E.
[49] I.S. Gill, A.-R. Azzouzi, M. Emberton, J.A. Coleman, E. Coeytaux, A. Scherz, P.T. Scardino, Randomized trial of partial gland ablation with vascular targeted phototherapy versus active surveillance for low risk prostate cancer: extended followup and analyses of effectiveness, J. Urol. 200 (2018) 786–793, https://doi.org/10.1016/j.juro.2018.05.121.
[50] V. Novohradsky, L. Markova, H. Kostrhunova, J. Kasparkova, J. Ruiz, V. Marchán, V. Brabec, A cyclometalated IrIII complex conjugated to a coumarin derivative is a potent photodynamic agent against prostate differentiated and tumorigenic cancer stem cells, Chemistry (2021), https://doi.org/10.1002/chem.202100568.
[51] T.G. St Denis, T. Dai, L. Izikson, C. Astrakas, R.R. Anderson, M.R. Hamblin, G.P. Tegos, All you need is light: antimicrobial photoinactivation as an evolving and emerging discovery strategy against infectious disease, Virulence 2 (2011) 509–520, https://doi.org/10.4161/viru.2.6.17889.
[52] N.A. Smith, P. Zhang, S.E. Greenough, M.D. Horbury, G.J. Clarkson, D. McFeely, A. Habtemariam, L. Salassa, V.G. Stavros, C.G. Dowson, P.J. Sadler, A.M.R. Combatting, Photoactivatable ruthenium(II)-isoniazid complex exhibits rapid selective antimycobacterial activity, Chem. Sci. 8 (2017) 395–404, https://doi.org/10.1039/C6SC03028A.
[53] W.-M. Ching, A. Zhou, J.E.M.N. Klein, R. Fan, G. Knizia, C.J. Cramer, Y. Guo, L. Que, Characterization of the fleeting hydroxoiron(III) complex of the pentadentate TMC-py ligand, Inorg. Chem. 56 (2017) 11129–11140, https://doi.org/10.1021/acs.inorgchem.7b01459.
[54] J. Ruiz, V. Rodríguez, N. Cutillas, A. Espinosa, M.J. Hannon, C. Novel, N-chelate platinum(II) antitumor complexes bearing a lipophilic ethisterone pendant, J. Inorg. Biochem. 105 (2011) 525–531, https://doi.org/10.1016/j.jinorgbio.2010.12.005.
[55] A.L. Spek, Structure validation in chemical crystallography, Acta Crystallogr. D 65 (2009) 148–155, https://doi.org/10.1107/S090744490804362X.
[56] M. Nishio, The CH/π hydrogen bond in chemistry. Conformation, supramolecules, optical resolution and interactions involving carbohydrates, Phys. Chem. Chem. Phys. 13 (2011) 13873–13900, https://doi.org/10.1039/C1CP20404A.
[57] M. Nishio, CH/π hydrogen bonds in crystals, CrystEngComm 6 (2004) 130–158, https://doi.org/10.1039/B313104A.
[58] M. Nishio, Y. Umezawa, K. Honda, S. Tsuboyama, H. Suezawa, CH/π hydrogen bonds in organic and organometallic chemistry, CrystEngComm 11 (2009) 1757–1788, https://doi.org/10.1039/B902318F.
[59] M. Nishio, Y. Umezawa, M. Hirota, The CH/π Interaction: Evidence, Nature, and Consequences, Wiley, 1998 accessed March 5, 2020, https://www.wiley.com/en-us/The+CH+%26pi%3B+Interaction%3A+Evidence%2C+Nature%2C+and+Consequences-p-9780471252900.
[60] Y. Umezawa, S. Tsuboyama, H. Takahashi, J. Uzawa, M. Nishio, CHπ interaction in the conformation of organic compounds, A database study, Tetrahedron. 55 (1999) 10047–10056, https://doi.org/10.1016/S0040-4020(99)00539-6.
[61] C. Janiak, S. Temizdemir, S. Dechert, W. Deck, F. Girgsdies, J. Heinze, M.J. Kolm, T.G. Scharmann, O.M. Zipffel, Binary [Hydrotris(indazol-1-yl)borato]metal complexes, M(Tp4Bo)2[1] with M = Fe, Co, Ni, Cu, and Zn: electronic properties and solvent-dependent framework structures through C–H···π interactions, Eur. J. Inorg. Chem. (2000) 1229–1241, https://doi.org/10.1002/(SICI)1099-0682(200006)2000:6<1229::AID-EJIC1229>3.0.CO;2-P, 2000.
[62] X.-J. Yang, F. Drepper, B. Wu, W.-H. Sun, W. Haehnel, C. Janiak, From model compounds to protein binding: syntheses, characterizations and fluorescence studies of [Ru II (bipy)(terpy)L] 2+ complexes (bipy = 2,2′-bipyridine; terpy = 2,2′:6′,2″-terpyridine; L = imidazole, pyrazole and derivatives, cytochrome c), Dalton Trans. (2005) 256–267, https://doi.org/10.1039/B414999H, 0.
[63] M. Dolores Santana, R. García-Bueno, G. García, M.J. Piernas, J. Pérez, L. García, I. López-García, Benzazolate complexes of pentacoordinate nickel(II). Synthesis, spectroscopic study and luminescent response towards metal cations, Polyhedron 61 (2013) 161–171, https://doi.org/10.1016/j.poly.2013.05.047.
[64] J. Cerezo, A. Requena, J. Zúñiga, M.J. Piernas, M.D. Santana, J. Pérez, L. García, Structure, spectra, and DFT simulation of nickel benzazolate complexes with tris(2-aminoethyl)amine ligand, Inorg. Chem. 56 (2017) 3663–3673, https://doi.org/10.1021/acs.inorgchem.7b00059.
[65] L. Bischoff, C. Baudequin, C. Hoarau, E.P. Urriolabeitia, Organometallic fluorophores of d8 metals (Pd, Pt, Au), in: P.J. Pérez (Ed.), Advances in Organometallic Chemistry, Academic Press, 2018, pp. 73–134, https://doi.org/10.1016/bs.adomc.2018.03.001.
[66] G. Ghosh, H. Yin, S.M.A. Monro, T. Sainuddin, L. Lapoot, A. Greer, S.A. McFarland, Synthesis and characterization of Ru(II) complexes with π-expansive imidazophen ligands for the photokilling of human melanoma cells, Photochem. Photobiol. 96 (2020) 349–357, https://doi.org/10.1111/php.13177.
[67] D. Trachootham, J. Alexandre, P. Huang, Targeting cancer cells by ROS-mediated mechanisms: a radical therapeutic approach? Nat. Rev. Drug Discov. 8 (2009) 579–591, https://doi.org/10.1038/nrd2803.
[68] R.R. Nazarewicz, A. Bikineyeva, S.I. Dikalov, Rapid and specific measurements of superoxide using fluorescence spectroscopy, J. Biomol. Screen 18 (2013) 498–503, https://doi.org/10.1177/1087057112468765.
[69] M.A. Chari, Zaied-A-Mosaa, D. Shobha, S. Malayalama, Synthesis of multifunctionalised 2-substituted benzimidazoles using copper (II) hydroxide as efficient solid catalyst, Int. J. Org Chem. 4 (2013) 243–250, https://doi.org/10.4236/ijoc.2013.34035.
[70] G.M. Sheldrick, Acta Crystallogr. A 64 (2008) 112–122.
[71] C.B. Hübschle, G.M. Sheldrick, B. Dittrich, J. Appl. Crystallogr. 44 (2011) 1281–1284.
[72] L. Krause, R. Herbst-Irmer, G.M. Sheldrick, D. Stalke, J. Appl. Crystallogr. 48 (2015) 3–10.
[73] K. Brandenburg, "DIAMOND Version 4.6.2. Copyright 1997-2019 Crystal Impact Gbr, Bonn, Germany," can be found under https://www.crystalimpact.com/diamond/, n.d.
[74] Z.F. Li, Y.W. Lam, A new rapid method for isolating nucleoli, in: R. Hancock (Ed.), The Nucleus, Springer, New York, NY, 2015, pp. 35–42, https://doi.org/10.1007/978-1-4939-1680-1_4.
[75] H. Huang, S. Banerjee, K. Qiu, P. Zhang, O. Blacque, T. Malcomson, M.J. Paterson, G.J. Clarkson, M. Staniforth, V.G. Stavros, G. Gasser, H. Chao, P.J. Sadler, Targeted photoredox catalysis in cancer cells, Nat. Chem. 11 (2019) 1041–1048, https://doi.org/10.1038/s41557-019-0328-4.
[76] F.-J. Ballester, E. Ortega-Forte, V. Porto, H. Kostrhunova, N. Davila-Ferreira, D. Bautista, V. Brabec, M.D. Santana, F. Domínguez, J. Ruiz, New half-sandwich ruthenium(II) complexes as proteosynthesis inhibitors in cancer cells, Chem. Commun. (2019) 1140–1143, https://doi.org/10.1039/C8CC09211G.
[77] F.J. Ballester, E. Ortega, D. Bautista, M.D. Santana, J. Ruiz, Ru(II) photosensitizers competent for hypoxic cancers via green light activation, Chem. Commun. 56 (2020) 10301–10304, https://doi.org/10.1039/D0CC02417A.
[78] E. Ortega, F.J. Ballester, A. Hernández-García, S. Hernández-García, M.A. Guerrero-Rubio, D. Bautista, M.D. Santana, F. Gandía-Herrero, J. Ruiz, Novel organo-osmium(II) proteosynthesis inhibitors active against human ovarian cancer cells reduce gonad tumor growth in Caenorhabditis elegans, Inorg. Chem. Front. 8 (2021) 141–155, https://doi.org/10.1039/C9QI01704F.